Mon. Not. R. Astron. Soc. **000**, 1–?? (2015) Printed 21 July 2015 (MN LaTeX style file v2.2)

arXiv:1507.05334v1 [astro-ph.CO] 19 Jul 2015

On Scale-Dependent Cosmic Shear Systematic Effects

T. D. Kitching[1]*, A. N. Taylor[2], M. Cropper[1], H. Hoekstra[3],
R. K. E. Hood[1], R. Massey[4,5], S. Niemi[1]
[1] *Mullard Space Science Laboratory, University College London, Holmbury St Mary, Dorking, Surrey RH5 6NT, UK*
[2] *SUPA, Institute for Astronomy, University of Edinburgh, Royal Observatory, Blackford Hill, Edinburgh, EH9 3HJ, UK*
[3] *Leiden Observatory, Leiden University, PO Box 9513, 2300 RA, Leiden, the Netherlands*
[4] *Institute for Computational Cosmology, Durham University, South Road, Durham DH1 3LE, UK*
[5] *Centre for Extragalactic Astronomy, Durham University, South Road, Durham DH1 3LE, UK*

ABSTRACT

In this paper we investigate the impact that realistic scale-dependence systematic effects may have on cosmic shear tomography. We model spatially varying residual ellipticity and size variations in weak lensing measurements and propagate these through to predicted changes in the uncertainty and bias of cosmological parameters. We show that the survey strategy – whether it is regular or randomised – is an important factor in determining the impact of a systematic effect: a purely randomised survey strategy produces the smallest biases, at the expense of larger parameter uncertainties, and a very regularised survey strategy produces large biases, but unaffected uncertainties. However, by removing, or modelling, the affected scales (ℓ-modes) in the regular cases the biases are reduced to negligible levels. We find that the integral of the systematic power spectrum is not a good metric for dark energy performance, and we advocate that systematic effects should be modelled accurately in real space, where they enter the measurement process, and their effect subsequently propagated into power spectrum contributions.

Key words: Cosmology: theory – large–scale structure of Universe

1 INTRODUCTION

Weak gravitational lensing is the effect whereby the image of a background object is distorted as a result of the intervening mass, causing tidal effects along the line of sight. An effect of weak lensing on the images of galaxies is to cause the third eccentricity (or third flattening) - colloquially referred to as 'ellipticity' - of the images to change. This change, to first order, in ellipticity is known as 'shear'. Galaxy images can be affected by shear distortions as a result of the gravitational potential around galaxies or clusters. They can also be affected by lensing from all scales in the cosmic web (large-scale structure) so that every galaxy is sheared by a very small amount; this is known as cosmic shear.

Cosmic shear is a particularly interesting phenomenon because the amplitude of the excess probability for any pair of galaxies to have aligned shear distortions – the correlation function – is related to the power spectrum of matter density perturbations, the growth of structure, and the distance-redshift relation. In this paper, and in the majority of the theoretical and methodological literature on cosmic shear the harmonic (Fourier) transform of the correlation function is used, which is known as the power spectrum. This statistic depends on several aspects of the cosmos that have a strong sensitivity to variations in cosmological parameters, and as a function of redshift. In particular cosmic shear is a statistic that is sensitive to changes in the dark energy equation of state.

Supplementing cosmic shear information with redshift information of galaxies is known as 3D cosmic shear (see Kitching et al., 2014 and references therein for an exposition). Cosmic shear 'tomography' is an approximation of 3D cosmic shear by assuming a fixed linear relation between the radial and azimuthal wavenumbers for the 3D shear field (the Limber approximation), and a binning in redshift (Kitching, Heavens, Miller, 2011). For a reviews of weak lensing and cosmic shear see for example Bartelmann & Schneider (2001), Hoekstra & Jain (2008) and Kilbinger (2014). In this paper we will focus on the requirements on systematic effects set when using cosmic shear tomography for cosmology.

Because cosmic shear can potentially measure the dark energy equation of state very accurately, there are several experiments either on-going, or planned, that will use cos-

---

* t.kitching@ucl.ac.uk

© 2015 RAS

mic shear. From the ground these are KiDS[1], DES[2], HSC[3], LSST[4], and from space *Euclid*[5] and *WFIRST-AFTA*[6].

The shear effect is a very small change in the ellipticity of a galaxy image: a change in the third flattening ('ellipticity') of approximately 10^{-2} (or, $\sim 10\%$ of the amplitude, which is approximately 10^{-1} on average). The measurement from data is complicated in several respects: even without the shear effect galaxy images would appear elliptical, there are 'intrinsic' ellipticity correlations (see Troxel & Ishak, 2014, Joachimi et al., 2015 for reviews); the measurement of ellipticity is affected by noise (Viola, Kitching, Joachimi, 2014) and modelling uncertainities (if a galaxy model is used, see for example Kitching et al., 2012; Voigt & Bridle, 2010); telescopes have an impulse-response, or point-spread-function (PSF) that blurs images (and, for ground-based telescopes, atmospheric effects further blur the images), and the PSF is typically also elliptical to some degree; and CCD detectors themselves can also degrade ellipticity as a result of radiation damage (CTI), manufacturing errors, or properties inherent to the devices. Therefore the control of systematic effects in experiments that wish to measure cosmic shear need to be characterised and accounted for in a rigorous manner.

There have been a number of studies of systematic effects that can degrade cosmic shear measurements (for example Massey et al., 2013; Kitching et al., 2009; Amara & Refregier, 2008; and references therein). These have typically looked at requirements either on an individual galaxy basis, or under the assumption that systematic effects are not dependent on angular scale (or a random dependency). Some exceptions include the galaxy ellipticity measurement simulations in Kitching et al. (2012) that investigated the change in power spectra from imperfect measurements, and Hoekstra (2004) who compared PSF modelling errors to the cosmic shear signal in data. Those studies that have included some scale-dependence have made an assumption that all systematic effects have scale-dependent functional behaviour that mimics a cosmological signal, the requirement used being an integral over all scales used in the analysis. This was the approach taken in Massey et al. (2013) and Cropper et al. (2013) that propagated requirements on systematic effects through to the performance on cosmological parameters.

In this paper we look at more realistic scenarios for the scale-dependence of systematic effects, on CCD detector, field-of-view, and larger scales. To realise a concrete version of these scales, we assume the baseline design of the Euclid hardware (Laureijs et al., 2011). We then propagate the expected angular behavior of systematic effects through to cosmic shear tomography cosmological parameter predictions. We also present a simple way to mitigate their impact by removing the scales at which the systematic has an effect.

The paper is presented as follows. In Section 2 we outline the basic methodology. In Section 3 we present some simple examples to demonstrate the main conclusions of the paper. In Section 4 we present some more realistic cases, and an application to charge transfer inefficiency requirements. In Section 5 we present some conclusions.

2 METHOD

The method we use is the following: we introduce realistic spatially varying systematics into our images, then measure the power spectra of these, and propagate them into the shear power spectra. We use the notation from Massey et al. (2013) and Cropper et al. (2013) where the observed tomographic cosmic shear power spectra $C^{\rm obs}_{ij,\ell}$ can be related to the true (systematic free) power spectra $C^T_{ij,\ell}$ given by

$$C^{\rm obs}_{ij,\ell} = (1 + \mathcal{M}_{ij,\ell})C^T_{ij,\ell} + \mathcal{A}_{ij,\ell} \quad (1)$$

where ℓ labels the angular wavenumber, and ij labels a redshift bin pair for which $i = [1, N_{\rm bin}]$. We consider in this expression a 'multiplicative' term $\mathcal{M}_{ij,\ell}$ and an 'additive' term $\mathcal{A}_{ij,\ell}$; here we label the redshift bin pair ij for generality, but for most of this paper we assume that they are redshift-independent effects and so do not use these labels. Equation (1) neglects mode-mixing that could contaminate E and B-mode power, intrinsic alignment terms (as shown in Kitching et al., 2012, Appendix A), and assumes that the multiplicative term is uncorrelated in ℓ (this term should be $\sum_{\ell'} \mathcal{M}_{\ell\ell'} C_{ij,\ell'}$, so we are assuming no off-diagonal terms in $\mathcal{M}_{\ell\ell'}$, we will investigate this further in future work). A 'systematic' power spectrum can then be defined as

$$C^{\rm sys}_{ij,\ell} = \mathcal{M}_\ell C^T_{ij,\ell} + \mathcal{A}_\ell. \quad (2)$$

The shear power spectrum can be related to the matter power spectrum $P(k; r(z))$, where k $h{\rm Mpc}^{-1}$ is a radial wavenumber and $r(z)$ is a comoving distance, and angular diameter distance through

$$C^T_{ij,\ell} = A \int_0^{r(z_H)} {\rm d}r' \frac{W_i(r')W_j(r')}{a(r')^2} P(\ell/r'; r[z]) \quad (3)$$

where $A = (3\Omega_{\rm M} H_0^2/2c^2)^2$ and $\Omega_{\rm M}$ is the dimensionless matter density, H_0 is the current value of the Hubble parameter, z_H is the redshift of the cosmic horizon, c is the speed of light in a vacuum, and $a(r)$ is the dimensionless scale factor. The weight function is $W_i(r) = \int_r^{r(z_H)} {\rm d}r' p(r'|r[z_i]) f_K(r' - r)/f_K(r')$, with i labelling a redshift bin, where $f_K(r) = \sinh(r)$, r, $\sin(r)$ for curvatures of $K = -1, 0, 1$, and $p(r'|r)$ is the probability that a galaxy with comoving distance r is observed at distance r'. This representation of the shear power spectrum assumes the Limber approximation, a spherical Bessel transform to comoving distance, and a binning in redshift. For a derivation of this from the full 3D cosmic shear power spectrum see Kitching, Heavens, Miller (2011).

2.1 Systematic Propagation

In Massey et al. (2013) and Cropper et al. (2013) the multiplicative and additive terms were linked to systematic changes in convolutive effects on the image (i.e. PSF effects and similar), non-convolutive effects (i.e. CTI effects and similar) and inaccuracies in the measurement of ellipticities. These papers looked at correlations of complex residuals $\langle\delta x \delta x^*\rangle$ where $\delta x = x_M - x_T$, the difference between the measured and true values of some quantity which is then decomposed into a bias and variance $\langle\delta x \delta x^*\rangle = \langle(x_M - \overline{x_M})^2\rangle + \langle(\overline{x_M} - x_T)^2\rangle = \sigma^2(x_M) + {\rm b}^2(x_M)$, where an bar denotes a mean quantity. Requirements can then be set on the bias and the variance that are functions of x_M. In this paper we expand the variance to the Fourier power spectrum of the variable, and treat the bias as a constant term. Massey et al. (2013) used an unconventional angle bracket notation when referring to the power spectra, as explained in Cropper et al. (2013).

---

[1] `http://kids.strw.leidenuniv.nl`
[2] `www.darkenergysurvey.org`
[3] `www.subarutelescope.org/Projects/HSC/`
[4] `http://www.lsst.org`
[5] `http://euclid-ec.org`
[6] `http://wfirst.gsfc.nasa.gov`

In this paper we are concerned with systematic effects that leave a residual, unknown pattern in the data that may occur after modelling and correction. We will focus on the residuals that may occur as a result of PSF measurement, CTI correction and shape measurement such that the variables that we model are: residual PSF ellipticity $\epsilon_{\rm PSF}$; residual PSF size measurements $R^2_{\rm PSF}$; residual CTI ellipticity $\epsilon_{\rm CTI}$; residual CTI size measurements $R^2_{\rm CTI}$; and systematic effects in shape measurement, μ and α, that contribute to the multiplicative and additive parts of the power spectrum respectively. Throughout we will refer to normalised sizes so that all quantities are divided by their mean values e.g. $R^2_{\rm PSF} = R^2_{\rm PSF,unnormalised}/\overline{R^2}_{\rm PSF,unnormalised}$. These quantities are related to the terms $\mathcal{A}$ and $\mathcal{M}$ in Massey et al. (2013), and are summarised in Cropper et al. (2013), which we reproduce in the following equations using the power spectrum notation. The multiplicative and additive terms have weighted contributions from the residual systematic effects given by

$$\begin{aligned}\mathcal{M}_\ell &= m_1\overline{R^2_{\rm PSF}} + m_2\overline{R_{\rm CTI}}\\ &+ m_3 R^{-4}_{\rm PSF} C_\ell^{R^2_{\rm PSF}} + m_4 R^{-2}_{\rm CTI} C_\ell^{R_{\rm CTI}}\\ &+ m_5\overline{\delta\mu},\end{aligned} \qquad (4)$$

and

$$\begin{aligned}\mathcal{A}_\ell &= a_1 C_\ell^{\epsilon_{\rm PSF}} + a_2 C_\ell^{\epsilon_{\rm CTI}}\\ &+ a_3 R^{-4}_{\rm PSF} C_\ell^{R^2_{\rm PSF}} + a_4 R^{-2}_{\rm CTI} C_\ell^{R_{\rm CTI}}\\ &+ a_5 C_\ell^{\alpha},\end{aligned} \qquad (5)$$

where overline denotes the mean of a quantity. In converting these quantities from the real-space notation to power spectra we note the following aspects. For constants (like the m_1 and m_2 terms), the Fourier transform results in a delta function, but the propagation through to multiplicative bias also involves a convolution. Carrying out the convolution turns them into constant multiplicative biases in the power spectra. The remaining terms, which still convolve C_ℓ, are then treated as diagonal, and hence ℓ-dependent multiplicative biases. The terms m_3 and m_4 in Cropper et al. (2013) only refer to errors, but as stated in Massey et al. (2013) they "[Ignore] a bias term in $\mathcal{M}$ proportional to the square of one already present (therefore negligible if the bias is small)", so these convert to C_ℓ terms, despite no bias being refered to.

The constants a_i and m_i can be derived from galaxy and instrumental properties, and have values, taken from Cropper et al. (2013), of: $a_1 = 0.1$, $a_2 = 0.74$, $a_3 = 0.001$, $a_4 = 0.0042$, $a_5 = 0.001$, and $m_1 = 1.20$, $m_2 = 0.34$, $m_3 = 0.18$, $m_4 = 0.015$, $m_5 = 1.20$. We note that there are two errata in Cropper et al. (2013) for the numerical values of the terms: $a'_4 = 4a'_3$ should be 0.004 not 0.0042, and $m'_4 = (m'_2)^2/4$ should be 0.007225 not 0.0075. These slightly increased values add some flexibility to the requirements by inceasing the contribution from these systematic effects to the overall systematic power spectrum, so we use the larger values in this paper. These expressions make the same assumptions as in Massey et al. (2013), that there is no correlation between systematics, and that some quantities are negligible with respect to others (for example the potential mode-mixing from correlations in μ).

We also note that the m_5 term in Cropper et al. (2013) could have read $m_5(\langle\delta\mu\rangle + (1/2)[\langle\delta\mu\rangle^2 + \sigma^2(\mu)])$ (propagating both terms from Cropper et al., 2013, equation 4, rather than only the $\langle m\rangle$ term). However as the $\sigma(\mu)$ term is assumed to be negligble (calibration emulations of data can be increased until this is the case), to linear order the term was used correctly and this is what we use in this paper. We have generalised the assessment of systematics to include scale-dependence, and we leave the investigation of these assumptions to future work.

2.2 Procedure

Given the equations (5) and (4) we can now assess the impact of spatially varying, scale-dependent, effects on cosmic shear tomographic power spectra. The procedure that we follow is the following:

(i) We create 2D residual ellipticity and size fields for each of the systematic effects. These can be any form, but in this paper we use prescriptions that mimic realistic scenarios.

(ii) We compute the power spectrum for each field. This uses the steps shown in Kitching et al. (2012) that take the Fourier transform of the field, rotate in Fourier space to an E/B mode frame, and take the average of the Fourier transform of the real part in shells in angular wavenumber ℓ.

(iii) We combine these power spectra using equations (5) and (4) to create additive $\mathcal{A}$ and multiplicative $\mathcal{M}$ functions.

(iv) We propagate the systematic power spectrum into Fisher matrix predictions to assess the change in cosmological parameter error (uncertainty), and bias, caused by the systematic.

2.3 Prediction Method

To compute expected cosmological parameter errors we use the Fisher matrix formalism presented in Hu (1999) for cosmic shear tomography. This results in a matrix $F_{\alpha\beta}$ (the Greek letters denote cosmological parameter pairs) where the $[(F^{-1})_{\alpha\alpha}]^{1/2}$ is a vector of expected, marginalised, cosmological parameter error. To compute the expected biases in cosmology parameters we use the formalism described in Kitching et al. (2009) where the predicted shift in a parameter α caused by a systematic effect is $b_\alpha = -(F^{-1})_{\alpha\beta}B_\beta$, where the vector B for each parameter β is $B_\beta = \sum_{ij,\ell}(1/\sigma^2_C)C^{\rm sys}_{ij,\ell}(\partial C_{ij,\ell}/\partial\beta)$ and the error on the power spectra σ_C is given in Hu (1999).

We use a CDM cosmology with a varying dark energy equation of state, where the free parameters are $\Omega_{\rm M}$, $\Omega_{\rm B}$, σ_8, w_0, w_a, h, n_s (respectively the dimensionless matter density;

dimensionless baryon density; the amplitude of matter fluctuations on 8Mpc scales – a normalisation of the power spectrum of matter perturbation; the dark energy equation of state parameterised by $w(z) = w_0 + w_a z/(1+z)$; the Hubble parameter $h = H_0/100\mathrm{kms}^{-1}\mathrm{Mpc}^{-1}$; and the scalar spectral index of initial matter perturbations). For each parameter we use the *Planck* maximum likelihood values (Planck, Paper XVI, 2013) about which we take derivatives of the power spectra for the Fisher matrix and bias vector. All parameter errors and biases we quote are marginalised over all other parameters in this set. We use the `camb sources`[7] code to compute the cosmic shear tomographic power spectra[8]. We use a maximum radial wavenumber of $k_{\max} = 5h\mathrm{Mpc}^{-1}$ and a corresponding redshift-dependent maximum ℓ-mode of $\ell = k_{\max} r[z]$.

The cosmic shear survey we assume is a *Euclid*-like experiment that has an area of 15,000 square degrees, a median redshift of $z_m = 0.9$, a number density of 30 galaxies per square arcminute, with a number density distribution $n(z)$ given in Taylor et al. (2006), and a photometric redshift probability distribution that is assumed to be Gaussian with a standard deviation of $\sigma(z) = 0.05(1+z)$. These characteristics are described in Laureijs et al. (2011), and are the same as those used in Massey et al. (2013). We assume that a field-of-view is 0.5 square degrees, covered by a 6×6 array of detectors, that are assumed to be four-side buttable (i.e. no gaps between the chips).

3 AN INVESTIGATION OF POWER SPECTRUM REQUIREMENTS

In Massey et al. (2013) requirements were set by Monte Carlo evaluation of the functional form of $\mathcal{A}_\ell$ and $\mathcal{M}_\ell$, and estimating the error, and bias, on the dark energy equation of state using the method described in Kitching et al. (2009). This found the "worst case" variation of these functions arising from the selection of a functional behaviour of $\mathcal{A}$ and $\mathcal{M}$ that most closely matched the derivative of the shear power spectrum with respect to the dark energy equation of state $\partial C_{ij,\ell}/\partial w_0$, with additional considerations arising because of the multiple tomographic bins and degeneracies with other cosmological parameters. Once this function was found the mean values of the $\mathcal{A}$ and $\mathcal{M}$ were computed and this was used to set requirement on PSF, CTI and shape measurement quantities through the weighting scheme in equations (4) and (5). The requirements on the mean integrated values[9] are: $\overline{\mathcal{A}} \leq 2.6\times10^{-7}$ and $\overline{\mathcal{M}} \leq 1.4\times10^{-2}$ using a maximum wavenumber of $\ell_{\max} = 5000$ to avoid the highly non-linear regime. A more stringent combined requirement on the integrated quantity[10] $(1/2\pi)\int \mathrm{d}\ell(\ell+1)C^{\mathrm{sys}}_{ij,\ell} \leq 10^{-7}$ was set by Amara & Refregier (2008), which they termed σ^2_{sys}.

This was a conservative approach to setting the requirement for systematic effects. In reality the propagation of systematic effects through to the dark energy equation of state depends on the amplitude, the total integral constraint of the systematic effects and the functional form in ℓ that the systematic effect causes.

3.1 Simple Examples

In Figure 1 we show an example of an additive Gaussian systematic power spectrum in ℓ, with a total integrated constraint of $\sigma^2_{\mathrm{sys}} = 10^{-7}$ (using an $\ell_{\max} = 20{,}000$). A wide range of biases meet this requirement. We find that a sharp high amplitude systematic effect in ℓ causes the largest bias, and a systematic with a slope of approximately unity in $\ell^2 C(\ell)$ has the smallest bias.

In a second test, in Figure 2 we show an ellipticity field with different real-space 2D spatial patterns: from a rectilinear pattern to a randomised pattern. In this case we find that the regular pattern produces the largest bias, whereas the smallest bias is caused by the randomised pattern.

In fact a systematic effect that has the same functional form as pure shot noise will, by definition, not cause any biases in the inferred cosmological parameters, but the error bar on those parameters will increase. A shot noise power spectrum is flat in ℓ-space, having equal power at all scales. In this case the systematic would add to the measured ellipticity shot noise, but we note that an unknown shot-noise-like component would still cause biases in the infered amplitude of the cosmic shear power spectra. We numerically test this in Figure 3 where we show that the bias is minimised when an additive systematic effect has a slope of zero i.e. is consistent with shot noise. This conclusion is also supported by the Figures 1 and 2.

3.2 Functional Sampling

In these tests we also find that the total integral constraint on the systematic power spectrum is in fact not a good metric. A single integral constraint can allow for dramatically different functional behaviour in the power spectra, and eventual biases: we can find example for which almost no cosmological parameter biases are introduced, but for which requirements of are not met using the published limits on this integral. This is because in previous studies functional forms were chosen by randomly sampling from truncated functional expansions. For example 200 bins in ℓ were used in Massey et al. (2014) and this is very unlikely to create an isolated spike in the reproduced power spectrum (a less than $1 : 10^{100}$ chance of producing a single ℓ-mode peak at a height of 90% of the maximum). We show this in Figure 4 where we do the same test as in Massey et al. (2014), but also supplement this with realisations that randomly sample from a Gaussian with a width chosen between $\sigma(\ell) = [0, 500]$ and a mean chosen between $[100, 5000]$. We find that indeed with a truncated functional expansion an integrated limit of $\sigma^2_{\mathrm{sys}} \leq 10^{-7}$ does ensure that dark energy biases are below bias/error= 1 (or the revised requirement of 0.31 used in Massey et al., 2014), but that a more thorough functional search, including power spectra with spike-like functional features can produce biases that are an order of magnitude larger.

These larger bias are caused because by spike-like fea-

---

[7] `http://camb.info/sources/`

[8] Matlab code to reproduce the results of this paper is available on request.

[9] From Cropper et al., 2013, where these are labelled $\mathcal{A}'$ and $\mathcal{M}'$.

[10] The integration limits were not defined for this quantity but in the text the range $10 < \ell < 2 \times 10^4$ was specified.

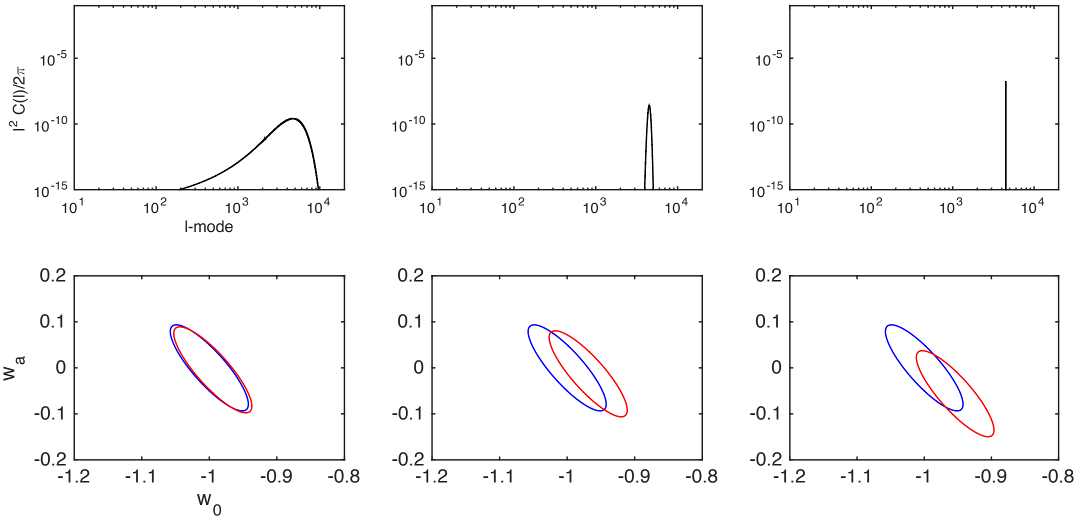

Figure 1. A simple example of the impact on the bias/error for the dark energy equation of state parameter w_0, for the survey parameters described in Section 2.3. The systematic functional form in ℓ is set to a Gaussian in ℓ centered on $\ell = 4500$ with three different full-width-half-maxima of 1000, 100 and 10 from right to left panels. The upper panels show the systematic power spectra: the y-axes are $\ell^2 C(\ell)/(2\pi)$ and the x-axes are ℓ-mode. The lower panels show the dark energy parameters with w_a on the y-axes and w_0 on the x-axes; the contours are 2-parameter 1-σ predicted confidence ellipses; the blue shows the systematic-free case and the red shows the case with the systematic effect.

tures because it is not in fact a worst case when whole functional form of $C_\ell^{\rm sys}$ resembles the sensitivity of the power spectrum with respect to a parameter, but instead a sufficiently large change in amplitude at a single ℓ-mode can cause a large bias. As an example consider fitting a straight line to some data points, one of which is offset by a very large amount: this would cause a bias in the fit of a gradient or offset despite only affecting a single data point (i.e. the systematic would not resemble the derivative of the model with resepct to either the gradient or offset at all data points). We note that the goodness of fit would be less in such a scenario, and indeed this could be measured to test if systematics are present, we leave this sophistication for future work.

We therefore conclude that integrated power spectrum requirements are not a good metric for dark energy performance. In Figure 2 we showed that the same integrated requirement can produce very different biases, and in Figure 4 we showed that sampling parameter values of a different functional form can result in dramatically different dark energy biases. Consequently we advocate here an approach where the systematic ellipticity field in real space is modelled, and the effect on the predicted cosmological inference propagated through a power spectrum estimation of that field. In this paper we look at realistic angular behaviour of systematics to investigate realistic cases, and assess at what level there is margin[11] in the requirements for cosmic shear tomography.

4 REALISTIC SCENARIOS

To investigate the impact that spatially varying systematic effects may have we begin by defining three realistic scenarios. In each case we model a representative 50 square degree patch of data, and assume that this pattern is repeated across whole survey area. These 50 square degrees are tiled with 10 arcsecond pixels which is the smallest angular scale that can be used in a cosmic shear analysis; this angular scale corresponds to radial scales (k-modes) of a few tens of Mpc^{-1} at the highest redshifts in a typical weak lensing survey (see Kitching & Taylor, 2010 for a discussion of this point). This is the same method that was used for Figure 2. Throughout we use a flat-sky approximation in the power spectrum analyses.

4.1 Experimental Setup

The three scenarios are meant to represent some extreme cases where uncertainty in the PSF and CTI modelling result in residuals that would formally not meet the requirements specified in Cropper et al. (2013). The scenarios also investigate different observing strategies. We do not explore

---

[11] A systems engineering term that means the difference between the requirement assumed during development/construction and the true/applicable requirement, a difference that typically leads to increased actual performance of an experiment over its design expectation.

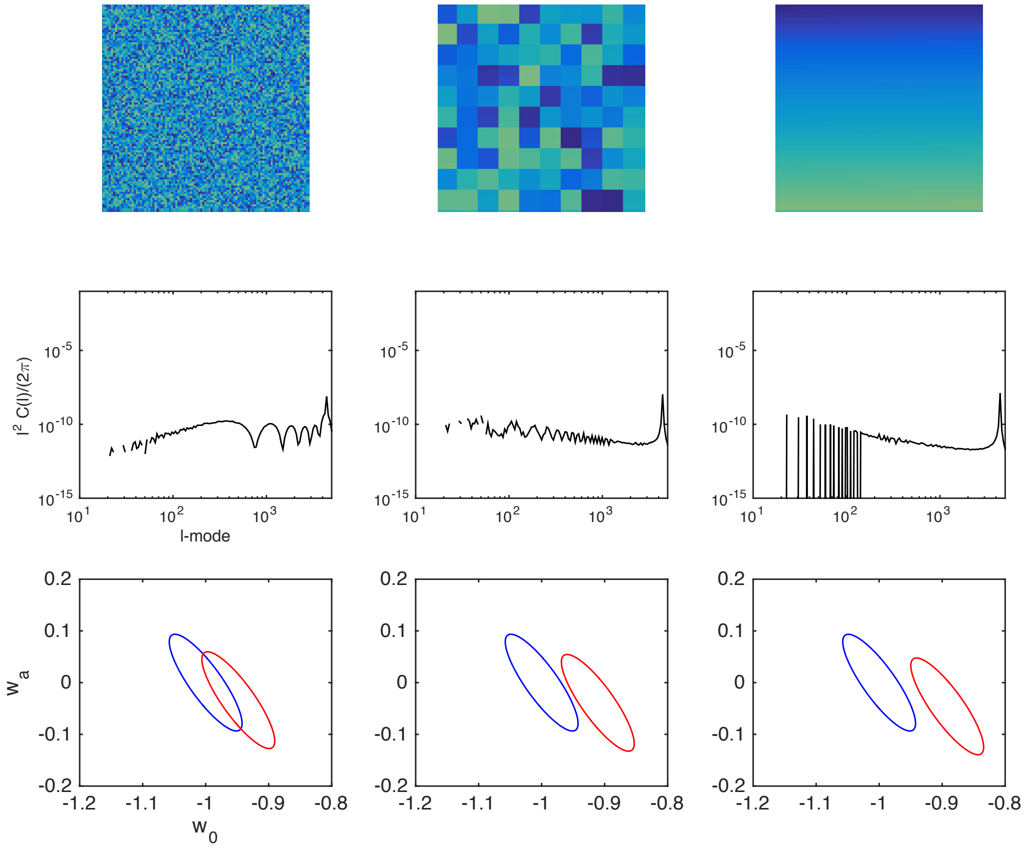

Figure 2. The upper panels show a simulated 50 square degree patch with a residual ellipticity field whose amplitude is represent by the colour (yellow is maximum blue is minimum). The middle row of panels show the power spectra of the systematic effects all normalised to have an integrated value of $\sigma^2_{\rm sys} = 10^{-7}$: the y-axes are $\ell^2 C(\ell)/(2\pi)$ and the x-axes are ℓ-mode. The lower panels show the impact on the dark energy parameters with w_a on the y-axes and w_0 on the x-axes; the contours are 2-parameter 1-σ predicted confidence ellipses, the blue shows the systematic-free case and the red shows the case with the systematic effect. The survey parameters are described in Section 2.3. The left column is the case where the field-of-view patches are observed in a random order, as the CTI increases linearly over the observation sequence; the middle panels show the case where 5 square degree patches are observed contiguously before moving on to a new 5 square degree patch at random; the right panels show the case that the full 50 square degrees are observed in a regular rectilinear scan, with no randomness in the tiling, and an increasing ellipticity. The spike in power at high-ℓ comes from the CCD scale.

all possible survey scenarios, but choose examples to highlight the flexibility of the modelling. The three ingredients in each scenario are as follows.

4.1.1 CTI Residual Modelling

Charge Transfer Inefficiency (CTI) is an effect caused in CCDs that are exposed to radiation. The radiation causes defects in the CCD in which electrons become trapped, which manifests itself as a blurred image in the readout direction of the CCD. Therefore the expected residuals should be limited to a CCD chip-scale and in the direction of the readout registers. To model the charge trailing due to CTI (see Massey et al., 2014), we use a model where a maximum residual ellipticity, or size, after correction is assigned at the center of a chip and linearly decreases to zero towards the chip edge. The amplitude of the maximum ellipticity, and the slope of the linear function can be changed on a chip-by-chip basis or over a field-of-view. The maximum ellipticity residual allowed due to imperfect corrective CTI modelling is taken from Cropper et al. (2013) to be 2.3×10^{-4}, and the maximum fractional size residual is set to 5×10^{-4} to match the maximum PSF size (although this requirement is not set in Cropper et al., 2013).

4.1.2 PSF Residual Modelling

To model residual ellipticity and size resulting from imperfect PSF modelling we use a polynomial of the form

$$\begin{aligned}\delta\epsilon_{\rm PSF} &= [c_0 + (c_1 x) + (c_2 y) \\ &+ (c_3 x^2) + (c_4 xy) + (c_5 y^2) \\ &+ (c_6 x^3) + (c_7 y^3)][1 + (c_8 x^2) + (c_9 y^2)]^{-1} \qquad (6)\end{aligned}$$

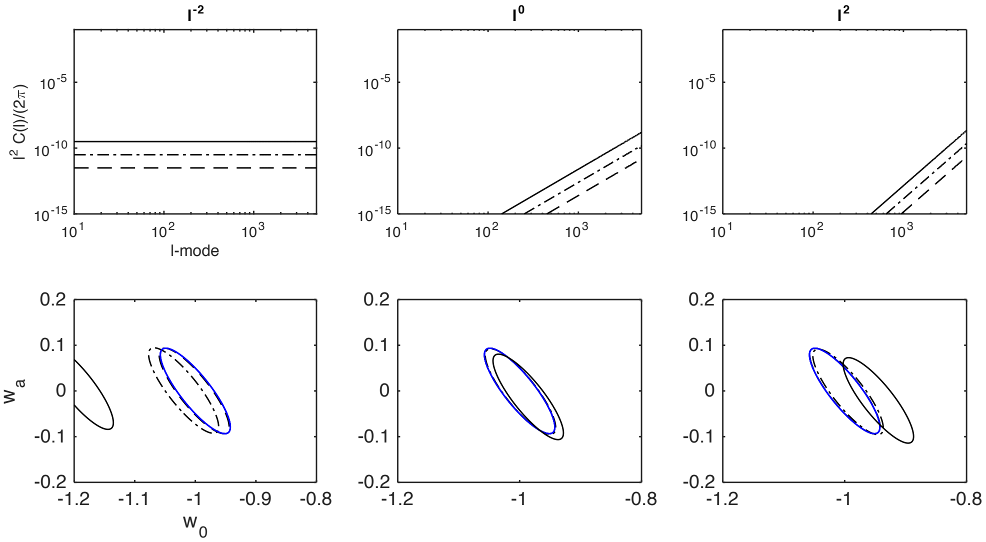

Figure 3. The upper panels show systematic power spectra, with a power-law functional form ℓ^n with slopes of $n = -2$, 0 and 2 as a function of ℓ-mode: the y-axes are $\ell^2 C(\ell)/(2\pi)$ and the x-axes are ℓ-mode. Three different integrated values of $\sigma^2_{\rm sys}$ are shown: $\sigma^2_{\rm sys} = 10^{-7}$ (dashed), $\sigma^2_{\rm sys} = 10^{-6}$ (dot-dashed) and $\sigma^2_{\rm sys} = 10^{-5}$ (solid). The lower panels show the dark energy parameters with w_a on the y-axes and w_0 on the x-axes; the contours are 2-parameter 1-σ predicted confidence ellipses, the blue shows the systematic-free case and the black shows the case with the systematic effect (dashed, dot-dashed and solid corresponding to the three cases in the upper panels). Where the contours used are not visible it is overlapping with the blue solid contour to within the thickness of the plotting line. The survey parameters are described in Section 2.3.

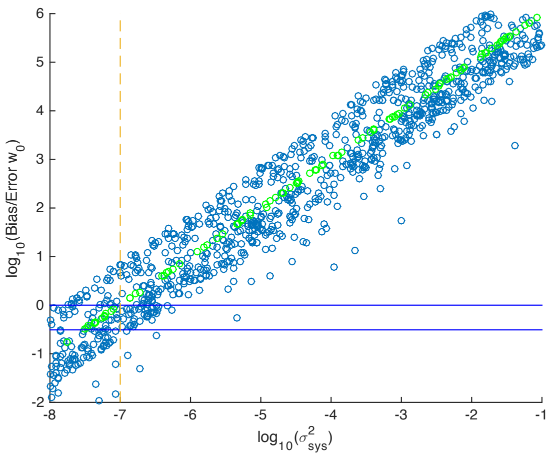

Figure 4. This Figure shows the impact that different functional forms for the systematic power spectrum have on the ratio of bias/error for the dark energy parameter w_0. The x-axes shows the integrated value of the systematic power spectrum $\sigma^2_{\rm sys}$, the y-axes shows the bias/error. The solid horizontal lines show bias/error= 1 and 0.31, the vertical (orange) dashed line shows $\sigma^2_{\rm sys} = 10^{-7}$. The blue dots show the range of biases found when taking 1000 realisations of the Guassian functional form described in Section 3.1. The green dots show the upper limit of the biases caused by realisations of a binned functional form in ℓ-mode (repeating the analysis of Massey et al., 2013). The survey parameters are described in Section 2.3.

from Hoekstra (2004) that looked at the impact of PSF variation on shear correlation functions, where x and y are Cartesian coordinates in the field-of-view. The size residuals are assumed to have the same spatial behaviour as those of the ellipticity, although this assumption could be relaxed. The coefficients are chosen to create PSF patterns that have features in them that may be expected from data shown in Section 4.2. The polynomial variation is scaled such that the maximum ellipticity residual in the PSF residuals is 1.1×10^{-4} from Cropper et al. (2013), and the maximum fractional size residual is 5×10^{-4}.

4.1.3 Shape Measurement Modelling

In the scenarios we investigate we assume that half of the survey can be observed with four exposures and half with three exposures; this is a pessimistic implementation of a fiducial Euclid survey (e.g. Amiaux et al., 2012). Biases in shape measurement are dominated by uncertainty in the signal-to-noise of the galaxy images (see for example Viola, Kitching, Joachimi, 2014), here we assume that residual uncertanties are a function of the initial bias and hence we simulate spatial variation in the multiplicative and additive parameters $\delta\mu$ and $\delta\alpha$ as being proportional to the number of exposures, that varies on field-of-view scales. The spatial variation is scaled such that the maximum values of these fields are 5×10^{-4} and 2×10^{-3} for α and $\delta\mu$ respectively (defined in Cropper et al., 2013).

We emphasise that these models are only examples, and that in fact any functional or non-parameter spatial behaviour could have been included in this analysis.

4.2 Scenarios

Using the descriptions from the previous section we examine three Scenarios with variations about these basic prescriptions, described in Table 1. These scenarios were chosen to represent extreme cases in survey design and systematics modelling. In particular the way that systematics evolve over the survey were taken to be constant, random or evolving which are distinct categories. Figures 5, 6 and 7 show the spatial patterns that the scenarios induce.

In Scenario 1 the CTI model and PSF model are constant for all fields-of-view: the values of the PSF coefficients used are $c_0=0.5$, $c_1=1.5$, $c_2=0.01$, $c_3=1.4$, $c_4=0.8$, $c_5=1$, $c_6=10$, $c_7=0.01$, $c_8=0.01$, $c_9=0.01$, the weighting function used is a checkerboard patter with alternative field-of-view having weights of 1 and 0.75. Scenario 2 has a different residual pattern for every field of view, which is randomly assigned: the CTI amplitude is chosen to be between zero and the requirement stated in Section 2, the weight functon is also randomly assigned a value of either 1 or 0.75 for each field-of-view, the PSF has a wider residual pattern with coefficient values $c_0=100$, $c_1=2.5$, $c_2=0.1$, $c_3=2.4$, $c_4=1000$, $c_5=1$, $c_6=200$, $c_7=0.1$, $c_8=0.1$, $c_9=0.1$. Scenario 3 has the PSF and CTI residual patterns changing slowly over the survey area: the CTI amplitude linearly increases between each field-of-view, starting with zero and increasing in stripes over the survey, the PSF amplitude decreases between each field-of-view, starting with the requirement value and decreasig to zero, the PSF model has coefficient values $c_0=0.5$, $c_1=2.5$, $c_2=0.1$, $c_3=2.4$, $c_4=100$, $c_5=1$, $c_6=20$, $c_7=0.1$, $c_8=0.1$, $c_9=0.1$, and the weight function has value of 1 and 0.75 arranged in stripes that are perpendicular to the direction over which the CTI and PSF change. These are realisations from a wide range of possible configurations that were chosen to be particulary extreme. We find that for all cases the dark energy Figure-of-Merit, $1/(\sigma(w_0)\sigma(w_a)-[\sigma^2(w_0,w_a)])$, is approximately 100, similar to that found in Laureijs et al. (2011) for cosmic shear tomography alone with 10 redshift bins centred on $[0.2,0.4,0.6,0.8,1.0,1.2,1.4,1.6,1.8,2.0]$.

Figures 5, 6 and 7 show the power spectrum from each component of the introduced systematic effects. It can be seen that the repeated spatial pattern of the systematics - on chip and field-of-view scales ($\ell_{\rm chip}\sim 2\pi/(0.5\pi/180/6)=4320$) - causes distinct features in the systematic power spectrum $C_\ell^{\rm sys}$ at these scales and their harmonics. The exact functional form depends on the distribution and the amplitude of the systematic effect modelled. Importantly in none of the extreme cases we consider does the systematic power spectrum mimic the derivative of the shear power spectrum with respect to any cosmological parameter. Hence in all three cases there is a small change in the predicted cosmological parameter errors, and bias, despite there being significant systematic effects in the modelled data. We find that, in agreement with the simple models in Section 3.1, systematic effects with an approximately shot-noise like power spectrum have a smaller bias. We also try filtering these scales, as we describe in Section 4.3.

The systematic effects that we simulate in this paper are all redshift independent. Therefore the primary impact they have is on w_0 which is a constant with redshift; w_a should be more affected by redshift-dependent systematic effects, and this is indeed seen in investigations on intrinsic alignments (see e.g. Kirk et al., 2015).

In Figure 5 the constant patterns produce variation only on the chip and field-of-view scales, hence the power spectra of the systematic effects are all at high-ℓ, and in the case of CTI localised at the chip scale, or multiples thereof. Therefore the removal of the chip scale power is particularly effective at removing bias. In Figure 6 the randomised nature of the systematic effects spreads the power over all scales. In particular it can be seen that the single spike in power due to CTI now has a broad shot noise-like component. These systematic power spectra therefore cause smaller biases, but the less clearly defined spike at the chip scale means that the removal of these modes is less effective. The removal of modes also increases the error bar, through the loss of information. In Figure 7 the regular field-of-view scale variation adds power at these scales, and the gradual changes over the entire field add power at low-ℓ.

The values of the integrated additive and multiplicative contributions in each of the scenarios are for Figures 5, 6, and 7 : $\overline{\mathcal{A}}=3.0\times10^{-6}$ and $\overline{\mathcal{M}}=1.0\times10^{-1}$, $\overline{\mathcal{A}}=2.9\times10^{-5}$ and $\overline{\mathcal{M}}=8.1\times10^{-2}$, and $\overline{\mathcal{A}}=3.4\times10^{-5}$ and $\overline{\mathcal{M}}=7.6\times10^{-2}$ respectively. These in some cases exceed the requirement set in Cropper et al. (2013) and Massey et al. (2013) despite the fact that the dark energy measurement would remain largely unaffected. This suggests that an improved set of requirements can be set, taking into account the expected spatial variation in the systematic effects. However we note that this can only be done once a model set up is evaluated for a particular experiment.

4.3 CTI Requirements

In each of the Figures 5, 6 and 7 we show the effect of removing power that is present around the CCD scale, and find that the dark energy biases are reduced in doing this. We now explore this ℓ-mode-filtering further within the context of the CTI systematic effect.

What the examples in Sections 3.1 and 4.2 show is that the dominant effect that causes a systematic bias in cosmic shear is the regularity (or stochasticity), of the spatially varying nature of the effect, that focuses power at particular frequency ranges in the power spectrum. To explore this further we consider requirements on one aspect of cosmic shear survey design: the amplitude of the detector CTI ellipticity residuals.

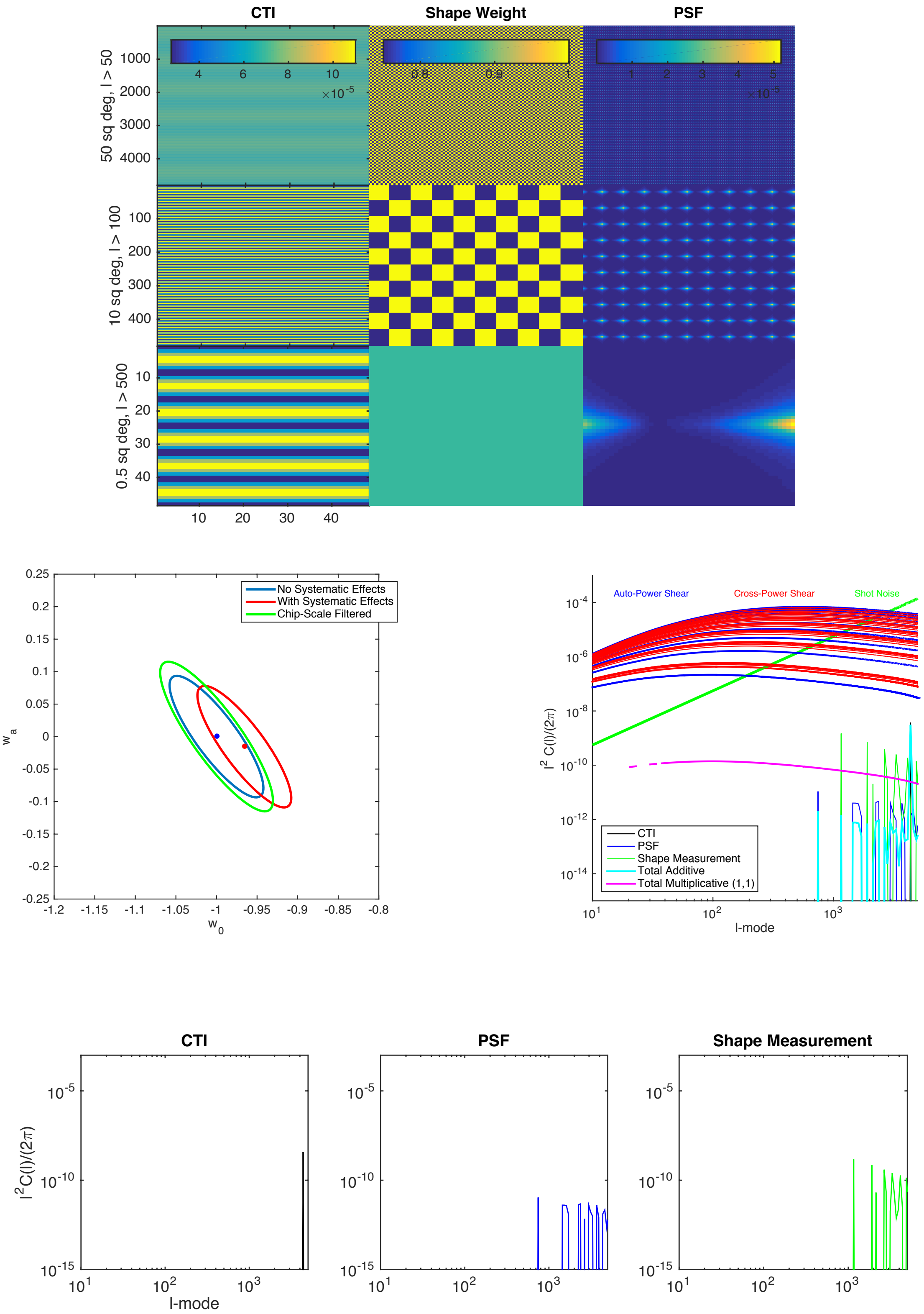

Figure 5. Scenario 1 systematic effects. The upper panels show the spatial variation in ellipticity for CTI, weighting and PSF (left to right), from top to bottom these are progressive zooms-in over 50 square degrees, 10 square degrees, and over 0.5 square degrees (a field-of-view); the size variations have a similar pattern. The middle right panel shows the power spectra for each ellipticity systematic effect, the cosmic shear tomography power spectra, and the per-ℓ-mode shot noise power spectrum. The total systematic power spectra are shown (both the additive $\mathcal{A}_\ell$ and multiplicative $\mathcal{M}_\ell$ terms) for the lowest redshift auto-correlation power spectra. In the middle left panel we show the predicted marginalised 2-parameter 1-σ error bars in the (w_0, w_a) plane with and without the systematic effects included for this case, and also in the case that the chip-scale ℓ-modes are filtered. The lower panels show the individual power spectra for each systematic effect. The survey parameters are described in Section 2.3.

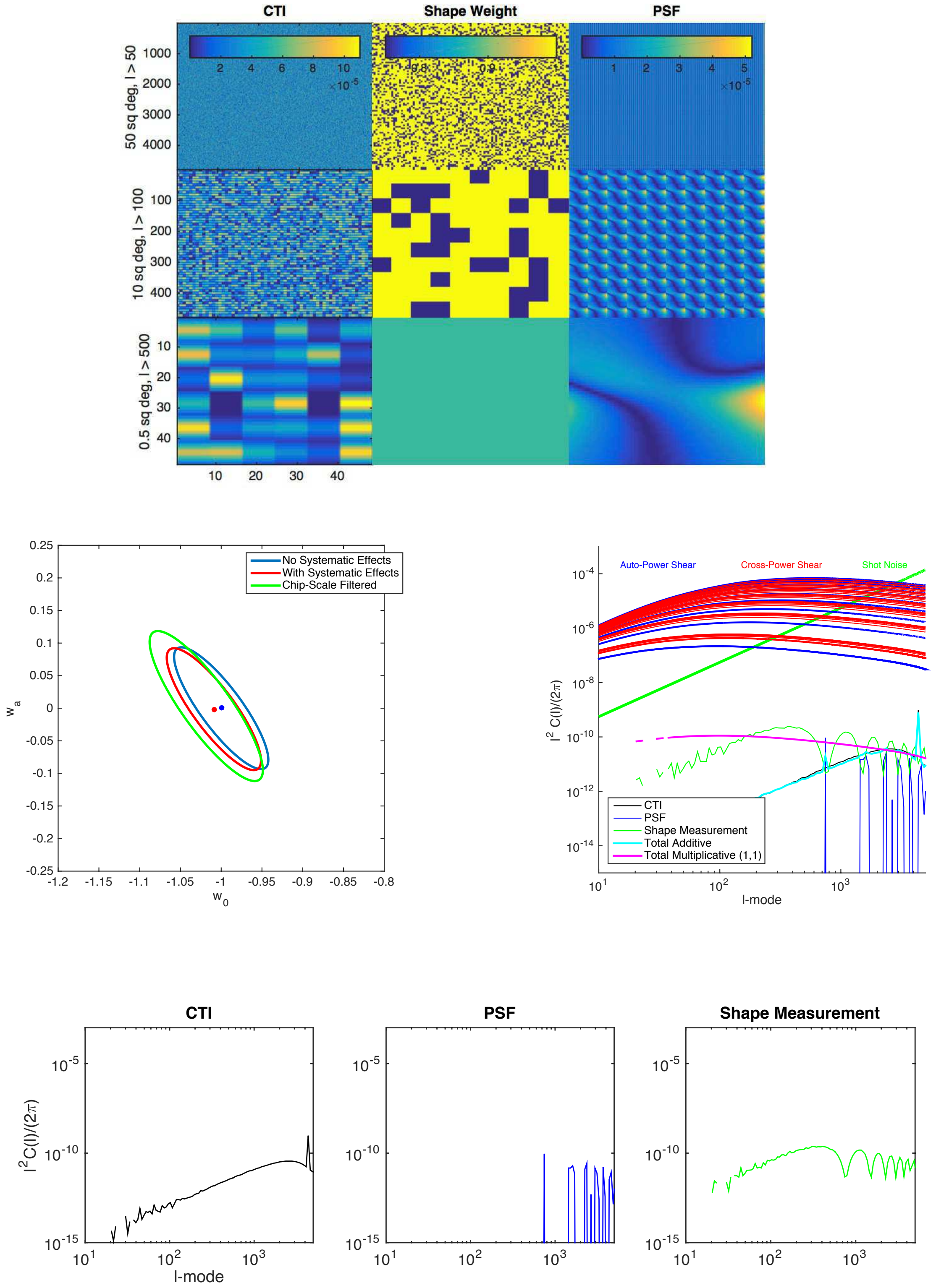

Figure 6. Scenario 2 systematic effects. The caption is the same as Figure 5.

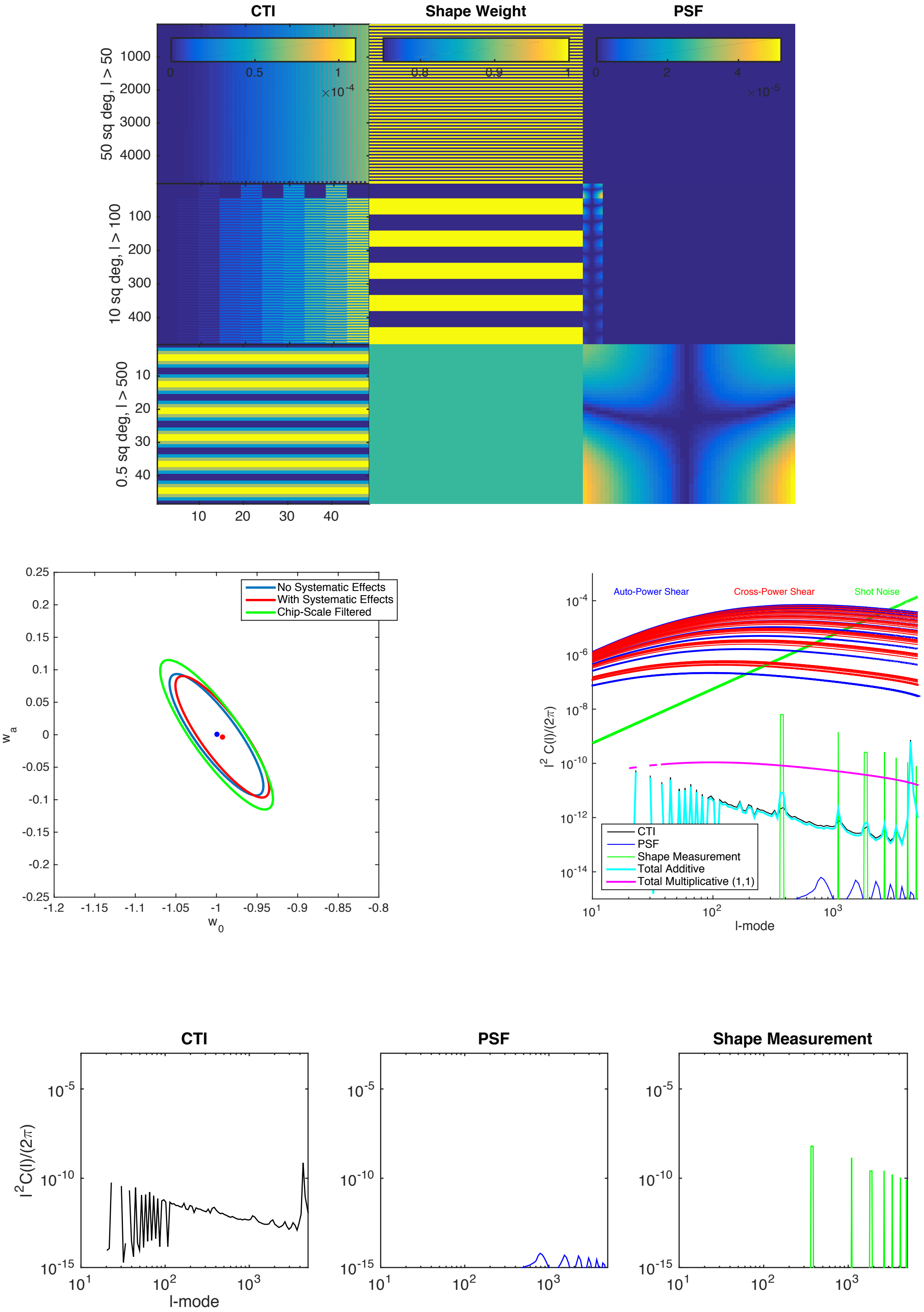

Figure 7. Scenario 3 systematic effects. The caption is the same as Figure 5.

	Scenario	**1) Constant Modelling**	**2) Randomised Model**	**3) FoV Evolution**
1.	CTI behaviour	Constant ∀ chip and FoV	Random amplitude	Increase in amplitude
2.	PSF behaviour	Constant & compact variation	Large random variation	Decrease in amplitude
3.	Field of View Tiling	Checkerboard	Random	Stripes

Table 1. The three example scenarios. The constant modelling scenario has no field-to-field variation of either CTI or PSF, and a checkerboard pattern of shape measurement weighting. In the randomised case the CTI, PSF and weighting vary randomly across the survey area. In the evolution case we assume a rectilinear scanning strategy over the 50 square degrees where the CTI gets progressively worse from the first to last field-of-view, and the PSF model gets progressively better. The PSF polynomial is chosen to represent a range of cases over the three scenarios as used in Figures 5, 6 and 7.

We set requirements on CTI by assuming a scenario where all the contribution to the total systematic additive bias comes from CTI only. These requirements will set an upper limit on the contribution of CTI to the total error budget on cosmic shear calculations. We assume that the CTI residual amplitude increases linearly in amplitude, similar to the "field-of-view evolution" scenarios in the previous section, and we vary the size of the patch over which the rectilinear scanning strategy is constant. We look at two cases, one where the full 50 square degrees is scanned in a rectilinear fashion, and one where the scanning strategy is entirely random. In each case the spatial arrangement of the fields is the same, so that the maxima and minima of the CTI pattern are the same, and it is only the order with which the fields are observed, and hence the amplitude of the CTI (which grows with time) that is different at different parts in the field. This is similar to the simple example given in Figure 2.

In Figure 8 we show how the bias on the dark energy equation of state varies with CTI amplitude for regular and randomised scanning strategies. We find, consistent with the previous results in this paper, that a randomised scanning strategy has a lower bias than a regular one. We also find that the requirement of 2.3×10^{-4} used in Cropper et al. (2013) is indeed a good level for this systematic effect. However, given that the CTI effect creates a sharply peaked systematic effect at the scale of the detector $\ell_{\rm chip}\approx 2\pi/(0.5\pi/180/6)=4320$ it should be possible to simply remove scales around this peak from the analysis to recover an unbiased estimate of cosmological parameters. We test this ℓ-mode-filtering by removing scales $\ell_{\rm chip}\pm 100$ from analysis. The dark energy Figure of Merit is reduced through the loss of information on these scales. However, this is still conservative as we could have allowed a coherent pattern in the detector frame that we then modelled instead of removed. In the absence of a model, the removal of these scales leads to a relatively modest reduction in Figure of Merit of 10%. In Figure 8 we show the impact of this filtering on the cosmology bias estimates. We find that for the case of a single 50 square degree patch the requirement on the CTI ellipticity amplitude is reduced by a factor of 9, In this case (as also shown in Figure 2) the power spectrum is sharply peaked at the chip-scale. For the randomised patch design the improvement is less, because the power is spread over a larger range of scales. Therefore we find that although a regularised survey design has a slightly larger bias, compared to a randomised pattern, the removal of scales affected by systematics can reduce biases. This however will only work for additive-type biases as the multiplicative bias acts as a convolution in Fourier space.

We explore the concept of ℓ-mode filtering further in Figure 9 where we show three examples where the CTI is 1) constant over the entire 50 square degrees – leading to a spike in the power spectrum at the chip scale; 2) evolves to reach a maximum after over 10% of fields are observed; 3) evolves to a maximum over the whole area. In this case we see that if the CTI is constant, then it is easily removed and leads to negligible parameter biases. In each plot the harmonics of the chip scale are outside the plotting and maximum ℓ-mode used. In the case that the CTI evolves, the power is spread from the chip-scale to the field-of-view scale, meaning it is more difficult to remove the contaminated scales, causing larger parameter biases. The difference in the power spectra between the second and third cases is very slight, an overall change in amplitude over most scales.

5 CONCLUSION

In this paper we investigated how spatially varying systematic effects can propagate into tomographic cosmic shear power spectra, and into the biases on the dark energy equation of state parameters w_0 and w_a inferred from these power spectra. This is a generalisation of previous studies that assumed systematics with no spatial variation (that affect all parts in a field-of-view equally), or random spatial variation. Many realistic systematics can be identified and nulled, and many residuals do not cause changes in the power spectrum that cause large biases in dark energy equation of state measurements. Consequently, both the previous approaches lead to requirements on weak lensing that are too stringent. Given that several surveys have been designed with these conservative assumptions in mind, this means that the expected performance is better or requirements can be relaxed (i.e. there is likely to be 'margin' in the design).

We find that the metric used to set requirements on systematic effects by e.g. Amara & Refregier (2008) and Massey et al. (2013) – namely the multiplicative and additive biases on the power spectrum integrated equally over all scales – do not account for the full story. These requirements can be exceeded in many realistic scenarios whilst the dark energy measurement can remain unbiased. This all assumes that a survey is driven by dark energy measurements, but a further aim may be measure power spectra for more general purposes. An additional point is that most of the biases we find are present on small scales ($\ell > 1000$) which are generally more difficult to model astrophysically (due to example baryonic feedback effects). So a cleaner cosmological probe both in terms of systematic effects and poor modelling may be one that removes such scale from an analysis and supple-

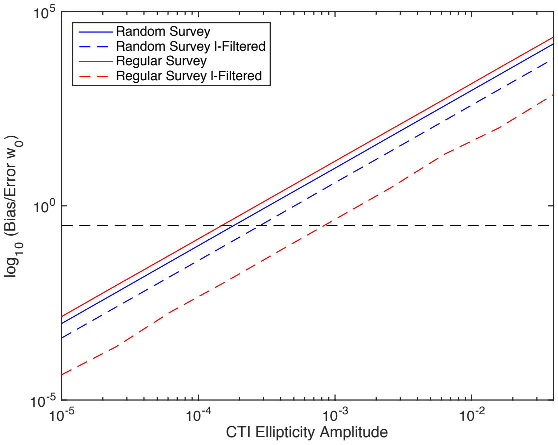

Figure 8. The change in dark energy parameter w_0 bias/error as a function of CTI ellipticity amplitude. Shown are solid lines with no ℓ-mode filtering and dashed lines with ℓ-mode filtering, for surveys that have a random surveying strategy (blue lines) and a rectilinear observing strategy (red lines). The horizontal dashed line shows the requirements from Massey et al. (2014) that the bias/error is less than 0.31. The survey parameters are described in Section 2.3.

ments the weak lensing with addition data (e.g. information from clusters).

Through a series of simplified examples we show that there is a trade-off between the spatial regularity of a systematic effect, its amplitude, and the integrated systematic power spectrum. A systematic effect that has a purely random spatial pattern acts to introduce shot-noise-like power to the cosmic shear, and as a result only slightly increases the cosmological parameter uncertainties – without causing a bias in the parameters. Conversely a very regular spatial pattern will cause sharply peaked features in the power spectrum, that can cause large biases but not impact the error bar. However if a systematic effect causes localised changes in the power spectrum, these are easy to remove by ignoring those ℓ-modes in a cosmological analysis; this is a conservative approach because one could also model these changes in the power spectrum.

We show three example scenarios that include modelling of CCD CTI effects, shape measurement error variation, and PSF modelling variation. These are extreme examples that serve to highlight that even in these cases the effect on dark energy equation of state measurements is small. We find that a significant contributor to bias in the dark energy equation of state comes from the survey observing pattern. If a survey has a randomised pattern of field-to-field weighting this acts to spread the systematic power over a larger range of scales. In contrast a rectilinear or striped pattern concentrates power on smaller scales that can be more easily filtered.

It should be noted however that throughout we make a number of simplifying assumptions, for example we do not include the effects of image ‘dithering’, and use a flat-sky approximation. The image dithering, and the use of multiple 50 square degree patches over the sky in the full survey, the phasing of the effects in each of which will not necessarily be maintained, will also qualify the effectiveness of the filtering. In particular a sharp spike-like feature on the chip-scale may be spread out over several ℓ-modes in a similar way to that seen in the randomised scenerio we investigate. In this case the filtering will become less effective, but the systematic itself will be closer to a randomised patterm which is likely to reduce bias in any case. We leave a full investigation of dithering effects for future work.

We use the formalism to investigate requirements on the amplitude of the CTI effect for cosmic shear. We find that in the case that the survey strategy is random, the contribution to the power spectrum is spread over a wide range in ℓ-mode and that the result from previous studies are recovered: that the ellipticity amplitude should be less than 2×10^{-4}. If the survey strategy is more regular then the systematic power spectrum is concentrated at a particular scale – with a larger amplitude – and causes larger biases. However because the systematic effect is very localised in ℓ-mode then a straightforward mitigation strategy is to remove those scales from a cosmological analyses and we find that such ℓ-mode-filtering reduces cosmological parameter biases relative to the randomised survey strategy case at the expenses of a 10% increase in the size of error bars.

The framework presented in this paper is a generalisation of investigations into systematic effects in cosmic shear surveys. Such a framework can be used to build more optimal survey strategies, and find margin in imaging survey specifications, potentially leading to less stringent requirements on the control of systematic effects in instrument and algorithmic design.

Acknowledgements: TDK and RM are supported by Royal Society University Research Fellowships. RM acknowledges the Science and Technology Facilities Council (grant number ST/H005234/1) and the Leverhulme Trust (grant number PLP-2011-003). Part of this work was an extension of the work presented in Hood (2014), a UCL Space Science and Engineering MSc thesis project (supervisor TDK).

REFERENCES

Amara, A., & Réfrégier, A. 2008, MNRAS, 391, 228
Amiaux, J., Scaramella, R., Mellier, Y., et al. 2012, Proc. SPIE, 8442, 84420Z
Bartelmann, M., & Schneider, P. 2001, physrep, 340, 291
Battye, R. A., Charnock, T., & Moss, A. 2014, arXiv:1409.2769

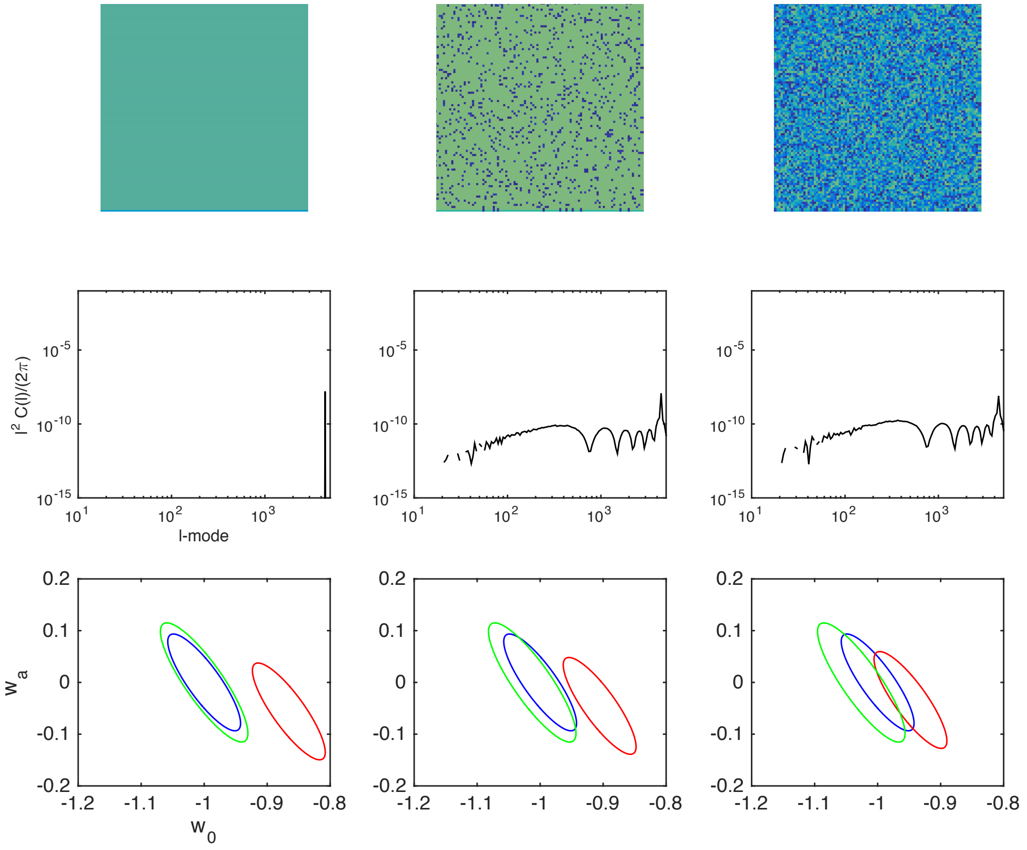

Figure 9. The top row of panels show three different cases where CTI amplitude changes over a 50 square degree patch, where the colour represents residual ellipticity amplitude caused by CTI (red high and blue small): the left hand panel where the CTI is the same over the whole patch; the middle panel where CTI is the same for 90% of the patch, and zero for the remainder; the right panel where the CTI amplitude randomly changes from field to field. The second row shows the corresponding power spectra for each systematic ellipticity field (the y-axes are $\ell^2 C(\ell)/(2\pi)$ and the x-axes are ℓ-mode). The lower panels show the expected errors in the (w_0, w_a) plane: the blue contours are with no CTI, the red contours with CTI, and the green contours with CTI and ℓ-mode filtering. The survey parameters are described in Section 2.3.

Cropper, M., Hoekstra, H., Kitching, T., et al. 2013, MNRAS, 431, 3103

Hoekstra, H., & Jain, B. 2008, Annual Review of Nuclear and Particle Science, 58, 99

Hu, W. 1999, apjl, 522, L21

Hood, R., UCL MSc Thesis, UCL; supervisor T. D. Kitching

Joachimi, B., Cacciato, M., Kitching, T. D., et al. 2015, arXiv:1504.05456

Kilbinger, M. 2014, arXiv:1411.0115

Kirk, D., et al. 2015, arXiv:1504.05465

Kitching, T. D., Amara, A., Abdalla, F. B., Joachimi, B., & Refregier, A. 2009, MNRAS, 399, 2107

Kitching, T. D., Heavens, A. F., & Miller, L. 2011, MNRAS, 413, 2923

Kitching, T. D., Balan, S. T., Bridle, S., et al. 2012, MNRAS, 423, 3163

Kitching, T. D., & Taylor, A. N. 2011, MNRAS, 416, 1717

Laureijs, R., et al. 2011, arXiv:1110.3193

MacCrann, N., Zuntz, J., Bridle, S., Jain, B., & Becker, M. R. 2014, arXiv:1408.4742

Massey, R., Hoekstra, H., Kitching, T., et al. 2013, MNRAS, 429, 661

Massey, R., Schrabback, T., Cordes, O., et al. 2014, MNRAS, 439, 887

Troxel, M. A., & Ishak, M. 2014, arXiv:1407.6990

Viola, M., Kitching, T. D., & Joachimi, B. 2014, MNRAS, 439, 1909

Voigt, L. M., & Bridle, S. L. 2010, MNRAS, 404, 458